

Hunting intermediate-mass black holes with LISA binary radial velocity measurements

Vladimir Strokov,^{1,*} Giacomo Fragione,^{2,3,†} Kaze W. K. Wong,^{4,‡} Thomas Helfer,^{1,§} and Emanuele Berti^{1,¶}

¹*Department of Physics & Astronomy, Johns Hopkins University*

²*Department of Physics & Astronomy, Northwestern University, Evanston, IL 60208, USA*

³*Center for Interdisciplinary Exploration & Research in Astrophysics (CIERA), Northwestern University, Evanston, IL 60208, USA*

⁴*Center for Computational Astrophysics, Flatiron Institute, New York, NY 10010, USA*

(Dated: September 20, 2021)

Despite their potential role as massive seeds for quasars, in dwarf galaxy feedback, and in tidal disruption events, the observational evidence for intermediate-mass black holes (IMBHs) is scarce. LISA may observe stellar-mass black hole binaries orbiting Galactic IMBHs, and reveal the presence of the IMBH by measuring the Doppler shift in the gravitational waveform induced by the binary’s radial velocity. We estimate the number of detectable Doppler shift events and we find that it decreases with the IMBH mass. A few Galactic globular clusters (including M22 and ω Centauri) may produce at least one event detectable by LISA if they harbor an IMBH at their center. We also estimate the number of expected Doppler shift events for IMBHs wandering in the Milky Way as a result of the disruption of their parent clusters. If there is at least one binary black hole orbiting around each wandering IMBH, LISA may detect tens of Doppler shift events from IMBHs wandering in our Galaxy, and produce a map of this elusive population.

I. INTRODUCTION

The existence of intermediate-mass black holes (IMBHs) is still controversial. While the boundaries between different classes of black holes are largely a matter of convention, IMBHs are usually assumed to have masses in the range $\sim 10^2 - 10^5 M_\odot$, filling the gap between stellar black holes (SBHs, with mass $\lesssim 100 M_\odot$) and supermassive black holes (with mass $\gtrsim 10^6 M_\odot$). Unlike their lighter and heavier counterparts, IMBHs remain elusive [1–3]. Finding IMBHs would have important implications for a wide range of phenomena, including the seeding of supermassive black holes, galaxy evolution, accretion, tidal disruption events, and gravitational waves (GWs) [4].

There are three main classes of proposed formation mechanisms for IMBHs [5]. The first predicts that IMBHs of $\sim 10^4 - 10^5 M_\odot$ are produced from the direct collapse of a metal-poor gas cloud, without passing through all the phases of stellar evolution [6, 7]. The second requires massive Population III stars, which can collapse to IMBHs of $\sim 100 M_\odot$ as a result of inefficient cooling [8–10]. The third involves dense star clusters, where an IMBH of mass $\sim 10^2 - 10^4 M_\odot$ can form either as a result of repeated mergers of SBHs, or from the collapse of a very massive star formed via stellar mergers [11–19].

Observational signatures of IMBHs are under intense scrutiny. Accreting IMBHs could be detected in galactic nuclei using observations ranging from the radio to the X-ray band, or as ultraluminous X-ray sources in the field [1, 20, 21]. The existence of nonaccreting IMBHs

can be inferred by tracking the orbits of stars and gas in their vicinity [22–24]. IMBHs that lurk in the centers of dense star clusters can interact and disrupt stars, resulting in detectable tidal disruption events, similar to those observed in galactic nuclei harboring supermassive black holes [3, 25]. Finally, the inspiral of a SBH into an IMBH and the merger of an IMBH binary could be detected with present and upcoming GW interferometers such as LIGO/Virgo/KAGRA, LISA, Cosmic Explorer and the Einstein Telescope. These systems are particularly interesting for multiband GW astronomy [26–28]. In particular, LISA will be able to observe IMBH–SBH binaries and IMBH binaries up to redshifts $z \sim 1-2$ [29–31]. The LIGO/Virgo Collaboration recently detected the first IMBH ever, the $\sim 150 M_\odot$ remnant from the GW190521 binary black hole (BBH) merger event [32], thus validating the expectation that GWs are uniquely well suited to finding IMBHs.

In this paper we explore the possibility of an *indirect* detection of IMBHs through LISA observations of GWs from stellar-mass BBHs. As pointed out in Ref. [33], and schematically illustrated in Fig. 1, the radial motion of a binary system orbiting a third, more massive body can produce Doppler shifts in the GW signal from the stellar-mass binary. These Doppler shift may be detectable by LISA (see also [34–37] for other applications of Doppler shift observations). Consider for example a BBH with component masses of $30 M_\odot$ orbiting a $10^3 M_\odot$ IMBH at a distance $R = 20$ AU: a few years before merger, LISA could measure the resulting Doppler shift in the GW signal as far as 16 Mpc at signal-to-noise ratio (SNR) of 100, and as far as 162.6 Mpc at SNR of 10, with a relative error $\sim 0.001\%$ and $\sim 0.01\%$, respectively [33].

Our main goal is to estimate the rates at which LISA could find IMBHs lurking in globular clusters (GCs) by measuring the radial velocity modulations in the GW signal of BBHs orbiting the IMBH. Most such BBHs are

* vstroko1@jhu.edu

† giacomo.fragione@northwestern.edu

‡ kwong@flatironinstitute.org

§ thelfer1@jhu.edu

¶ berti@jhu.edu

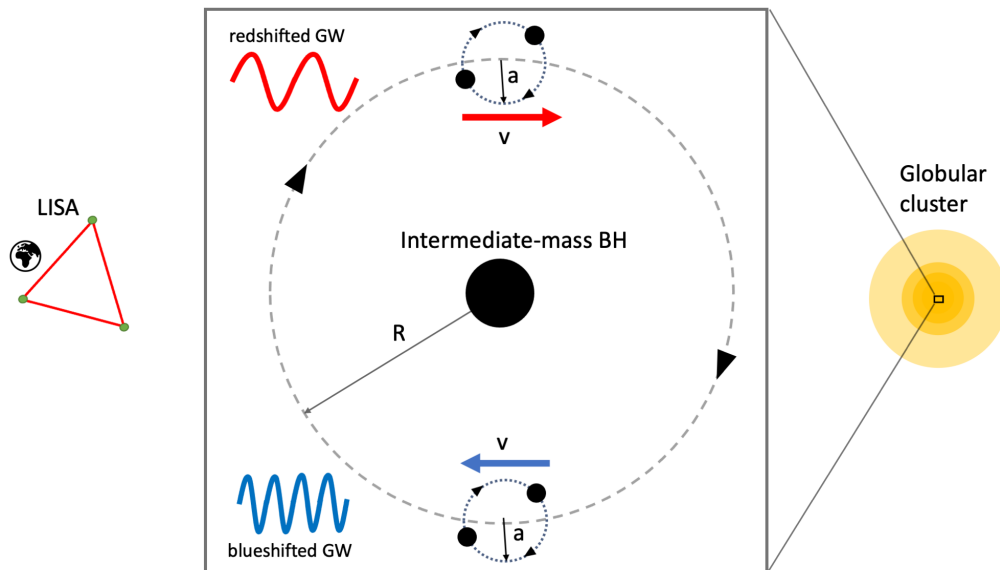


FIG. 1. Schematic illustration of the IMBH detection method explored in this paper. The radial motion of a BBH orbiting an IMBH located in a GC causes a periodic Doppler shift – either a redshift or a blueshift – in the GW signal observed by LISA. The detection of the Doppler shift can be used to infer the presence of the IMBH.

far from merger, and LISA can only measure the Doppler modulation if they are within ~ 100 kpc (that is, within the Milky Way). In this paper, we first estimate the rates of IMBH detections via LISA radial velocity measurements by using catalogs of the observed population of GCs in the Milky Way. Then we ask whether the radial velocity method could spot IMBHs that are wandering in the Galaxy, being left behind as a result of the disruption of their parent clusters.

The paper is organized as follows. In Sec. II we present our waveform model and parameter estimation method, and in Sec. III we describe our astrophysical models. In Sec. IV we report our results for the number of detectable Doppler shift events, both in Galactic GCs and in the neighborhoods of wandering IMBHs. Finally, in Sec. V we summarize our conclusions and discuss possible directions for future work. Throughout this paper we use geometrical units ($G = c = 1$).

II. WAVEFORM MODEL AND PARAMETER ESTIMATION

In order to take into account the Doppler shifts in a GW signal, we start off with the frequency-domain expression for the gravitational waveform from a BBH of component masses m_1 and m_2 :

$$h_{\alpha}^{(0)}(f) = \frac{\sqrt{3}}{2} A(t) \mathcal{A} f^{-7/6} e^{i[\Psi(f) - \varphi_p(t) - \varphi_D(t)]}, \quad (1)$$

where

$$A = \sqrt{\frac{5}{96}} \frac{\mathcal{M}^{5/6}}{\pi^{2/3} D_L}, \quad (2)$$

the index $\alpha = I, II$ denotes the two independent interferometric responses in the LISA arms [38], f is the GW frequency, $\mathcal{M} = \eta^{3/5}(m_1 + m_2)$ is the chirp mass, $\eta = m_1 m_2 / (m_1 + m_2)^2$ is the symmetric mass ratio, and D_L is the luminosity distance. The amplitude $A(t)$, polarization phase $\varphi_p(t)$ and Doppler phase $\varphi_D(t)$, where $t = t(f)$, arise from the geometry of the interferometer and from its motion around the Sun [38]. They can be expressed in terms of the sky position angles ($\bar{\theta}_S, \bar{\phi}_S$) of the BBH with respect to the Solar System, and the orientation angles ($\bar{\theta}_L, \bar{\phi}_L$) of the BBH's orbital angular momentum. For the functions $\Psi(f)$ and $t = t(f)$, which encode the inspiral dynamics of the BBH under gravitational radiation reaction, we use expansions up to second post-Newtonian (2PN) order, assuming for simplicity that the binary components are nonspinning [39]. Without loss of generality, we set the coalescence time t_c and the coalescence phase ϕ_c to zero. We collectively denote all parameters entering Eqs. (1) and (2) as the components of a vector $\theta_a \equiv \{\mathcal{M}, \eta, D_L, t_c, \phi_c, \bar{\theta}_S, \bar{\theta}_L, \bar{\phi}_S, \bar{\phi}_L\}$.

Let us now consider the case where the BBH orbits an IMBH of mass M_{IMBH} on a circular orbit of semi-major axis R and inclination I with respect to the plane of sky. The Doppler shift due to the motion of the binary gives rise to a correction to the phase. As long as the frequency of the GW signal changes slowly compared to the orbital period P of the binary around the IMBH, the resulting waveform reads [33]

$$h_{\alpha}(f; \tilde{\theta}_1) = h_{\alpha}^{(0)}(f; \theta_a) \exp\left\{ \left[i f v_{\parallel} P \sin\left(\frac{2\pi t(f)}{P}\right) \right] \right\}. \quad (3)$$

Here P is the BBH orbital period around the IMBH,

$$P = 2\pi \sqrt{\frac{R^3}{M_{\text{tot}}}} = 1 \text{ yr} \left(\frac{R}{10 \text{ AU}} \right)^{3/2} \left(\frac{M_{\text{tot}}}{10^3 M_{\odot}} \right)^{-1/2}, \quad (4)$$

with $M_{\text{tot}} = M_{\text{IMBH}} + m_1 + m_2$, and v_{\parallel} is the amplitude of the radial velocity

$$v_{\parallel} = \frac{2\pi R \sin I}{P} \frac{M_{\text{IMBH}}}{M_{\text{tot}}} = 300 \text{ km s}^{-1} \left(\frac{R \sin I}{10 \text{ AU}} \right) \left(\frac{P}{1 \text{ yr}} \right)^{-1} \left(\frac{M_{\text{IMBH}}}{M_{\text{tot}}} \right). \quad (5)$$

The extended set of waveform parameters $\tilde{\theta}_a$ now includes both v_{\parallel} and P , i.e. $\tilde{\theta}_a = \theta_a \cup \{v_{\parallel}, P\}$. The choice of the initial orbital phase is irrelevant as long as the observation time $T_{\text{obs}} > P$.

To estimate the relative errors $\Delta v_{\parallel}/v_{\parallel}$ and $\Delta P/P$ we use the Fisher matrix method (see e.g. [39, 40]). In our particular case, the Fisher matrix Γ_{ab} and SNR read

$$\Gamma_{ab} \equiv 4 \text{Re} \sum_{\alpha=I,II} \int_{f_0}^{f_0+\delta f} \frac{\partial h_{\alpha}^*}{\partial \tilde{\theta}_a} \frac{\partial h_{\alpha}}{\partial \tilde{\theta}_b} \frac{df}{S_n(f)}, \quad (6)$$

$$\text{SNR} = \left[4 \sum_{\alpha=I,II} \int_{f_0}^{f_0+\delta f} \frac{|h_{\alpha}|^2 df}{S_n(f)} \right]^{1/2}, \quad (7)$$

where $S_n(f)$ denotes the LISA noise power spectral density [41]. Here we use the noise power spectral density $S_n(f)$ corresponding to the LISA Science Requirements Document (SciRD), corrected for the ‘‘de-averaging’’ factor of 3/20, and including the foreground of Galactic white dwarf binaries corresponding to 4 years of observation. The errors in the parameters are given by the diagonal terms of the correlation matrix (the inverse of the Fisher matrix), i.e. $\Delta \tilde{\theta}_a = (\Gamma^{-1})_{aa}$ (no summation implied). In the equations above, f_0 is the GW frequency at the beginning of the BBH observation, and δf is the change in frequency during the observation time. Given an expression for $t(f)$, as discussed below Eqs. (1) and (2), the change in frequency can be found from $t(f_0 + \delta f) - t(f_0) = T_{\text{obs}}$, where we assume $T_{\text{obs}} = 4 \text{ yr}$ to be the nominal observation time for LISA [42] (see [43] for a discussion of different options for the mission duration).

Since the BBHs under consideration are usually observed long before merger, typically $\delta f/f_0 \ll 1$. This means that we must be careful to evaluate the integral in Eq. (6) with sufficient accuracy. Indeed, the integrand γ_{ab} is a sum of two direct vector products: $\gamma_{ab} \propto \partial_a \hat{h} \partial_b \hat{h} + \hat{h}^2 \partial_a \phi \partial_b \phi$, where $\hat{h} \equiv |h_{\alpha}|/\sqrt{S_n}$ and $\phi = \arg h_{\alpha}$. Therefore, if we expand Γ_{ab} to first order in δf , $\det\{\Gamma_{ab}\} \propto (\delta f)^N \det\{\gamma_{ab}\} = 0$, where N is the number of parameters ($N = 11$ in our case). This makes the determinant at least $\mathcal{O}((\delta f)^{N+1})$, and special care is required when inverting the matrix. We use the Python library `mpmath` [44] for arbitrary precision arithmetic, setting the number of significant digits equal to 75.

III. ASTROPHYSICAL SCENARIOS

In this section we introduce some astrophysical models to estimate the number of systems that yield detectable Doppler shifts. We consider two scenarios. In the first (Sec. III A), BBHs orbit IMBHs located in Galactic GCs. In the second (Sec. III B), they orbit wandering IMBHs left behind when clusters dissolve by losing their mass due to tidal stripping by the Galaxy, stellar evolution, and star ejections.

A. Intermediate-mass black holes in Milky Way globular clusters

In our first scenario, we consider IMBHs that may be located at the center of Galactic GCs. We extract GC parameters (luminosities, angular positions, distances, and metallicities) from the 2010 edition of the Harris catalog¹ [45]. We only exclude the cluster GLIMPSE02, since its absolute magnitude (as well as many other parameters) is not reported. In order to convert absolute visual magnitudes to cluster masses, we assume a mass-to-light ratio of $1.5 M_{\odot}/L_{\odot}$ [46]. Note that this value is close to the typical value derived from a sample of the Milky Way GCs [47, 48], although some models could yield higher mass-to-light ratios [49].

For simplicity, we assume that every cluster hosts an IMBH in its center, with a mass making up a fixed fraction

$$f_{\text{IMBH}} = \frac{M_{\text{IMBH}}}{M_{\text{GC}}} \quad (8)$$

of the cluster mass M_{GC} . Motivated by observational constraints on the masses of IMBH candidates, and in order to bracket the uncertainties on estimated IMBH masses in GCs (see e.g. Table 3 in [4]), we explore the range of mass fractions $f_{\text{IMBH}} = 10^{-3} - 10^{-1.5}$, which corresponds to 0.1%–3.2% of the host GC mass. As long as calculating this fraction results in a black hole of $> 100 M_{\odot}$, we consider it to be an IMBH and use it in the rest of the simulation.

To obtain the masses m_1 and m_2 of the BBH components orbiting the IMBH, we first sample the masses of their stellar progenitors from a Kroupa initial mass function [50]

$$\xi(m_*) = k_1 \begin{cases} \left(\frac{m_*}{0.5}\right)^{-1.3} & 0.08 \leq m_*/M_{\odot} \leq 0.50, \\ \left(\frac{m_*}{0.5}\right)^{-2.3} & 0.50 \leq m_*/M_{\odot} \leq 100.0, \end{cases} \quad (9)$$

where $k_1 \approx 0.62$. We evolve stars with mass $m > 20 M_{\odot}$ using the latest version of SSE [51, 52], updated with the most up-to-date prescriptions for stellar winds and remnant formation, until they form an SBH. Stellar tracks

¹ Available at <https://physics.mcmaster.ca/~harris/mwgc.dat>

are computed using the metallicity appropriate to each GC in the Milky Way. For clusters with no estimated value of the metallicity, we set it equal to the average catalog metallicity $\bar{Z} = 0.05 Z_{\odot}$, where $Z_{\odot} \approx 0.02$ is the solar metallicity [53].

Next, we randomly combine pairs of SBH remnants to form BBHs. For each BBH, we draw its semi-major axis a from a log-uniform distribution between $a_{\min} = 0.01$ AU and $a_{\max} = 100$ AU, while the semi-major axis R of its orbit around the central IMBH is drawn from a uniform distribution in the range $[0, r_{\text{infl}}]$. Here r_{infl} is the influence radius of the IMBH, related to the the GC half-mass radius r_{h} by

$$r_{\text{infl}} = f_{\text{IMBH}} r_{\text{h}}. \quad (10)$$

In turn, the half-mass radius is computed using the following expression for the half-mass density [54]:

$$\rho_{\text{h}} = 10^3 \frac{M_{\odot}}{\text{pc}^3} \min \left\{ 100, \max \left[1, \left(\frac{M_{\text{GC}}}{2 \times 10^5 M_{\odot}} \right)^2 \right] \right\}. \quad (11)$$

When we sample a and R , we check that the triple system (BBH+IMBH) is stable under the tidal disruption condition [55–57]

$$\frac{R}{4r_{\text{t}}} > 1, \quad (12)$$

where

$$r_{\text{t}} = 0.05 \text{ AU} \left(\frac{a}{0.01 \text{ AU}} \right) \times \left(\frac{M_{\text{IMBH}}}{10^3 M_{\odot}} \right)^{1/3} \left(\frac{m_1 + m_2}{20 M_{\odot}} \right)^{-1/3} \quad (13)$$

is the tidal disruption radius. Finally, the orientations of both the BBH’s orbital angular momentum and of the BBH orbit around the IMBH are assumed to be distributed isotropically: the direction of the orbital angular momentum $\mathbf{n}_L \equiv (\sin \bar{\theta}_L \cos \bar{\phi}_L, \sin \bar{\theta}_L \sin \bar{\phi}_L, \cos \bar{\theta}_L)$ points to a random direction on the sphere, and $\cos I$ is distributed uniformly in the range $[-1, 1]$.

Typically, $\mathcal{O}(10)$ BBHs lurk in a star cluster at any given time [58, 59]. However, this number could significantly change under the assumption of high primordial binary fractions and/or for a top-heavy initial mass function – in particular, in the case where massive black holes are formed [18, 60] – or in the case of core-collapse star clusters [61]. To bracket these uncertainties, we consider two possibilities for the number of BBHs in a catalog. In Sec. IV we refer to these possibilities as the cases of “many” and “few” BBHs, by which we mean that a star cluster hosts $\mathcal{O}(100)$ or $\mathcal{O}(10)$ BBHs.

In our models, we sample the respective number of BBHs using the procedure outlined above and select only those emitting in the LISA band, i.e. those with GW frequency $2/P_{12} > 10^{-5}$ Hz, where P_{12} is the period of the binary. The results for the number of BBHs with detectable Doppler shifts are reported in Sec. IV A below.

B. Wandering intermediate-mass black holes

In the second scenario, we explore the possibility that BBHs may orbit around wandering IMBHs. During their evolution, some of the clusters dissolve by losing their mass due to tidal stripping by the Galaxy, stellar evolution, and star ejections [54], in which case they may leave behind the IMBHs that were hosted in their centers [25, 30].

To estimate how many of these wandering IMBHs could be revealed by the method of radial velocities, we start off by simulating the evolution of GCs in the Milky Way [31, 54]. Initially, GCs are assumed to comprise a fraction $f_{\text{GC}} = 0.01$ of the Milky Way’s mass $M_{\text{gal}} = 5 \times 10^{10} M_{\odot}$ (approximately equal to the estimated stellar mass [62]), and their masses are sampled from the distribution

$$F(M_{\text{GC}}) \propto M_{\text{GC}}^{-2} \exp \left\{ \left(-\frac{M_{\text{GC}}}{10^6 M_{\odot}} \right) \right\} \quad (14)$$

in the range $[10^4 M_{\odot}, 10^7 M_{\odot}]$. The initial distribution of GC distances to the Galactic center is assumed to follow a spherical Sérsic profile [63] with total stellar mass M_{gal} , effective radius $r_e = 4$ kpc, and concentration index $n_s = 2.2$. When computing GC orbits in the Galaxy, we also include the contribution of the gravitational potential of dark matter, described by a Navarro–Frenk–White profile [64] with total mass $M_{\text{h}} = 10^{12} M_{\odot}$, scale radius $r_s = 20$ kpc, and virial radius $R_{\text{vir}} = 10 r_s$.

The initial cluster positions change in time because of dynamical friction, so that their distance r to the Galactic center decreases in accordance with equation

$$\frac{dr^2}{dt} = -\frac{r^2}{t_{\text{df}}(r)}, \quad (15)$$

where

$$t_{\text{df}} = 0.45 \text{ Gyr} \left(\frac{r}{\text{kpc}} \right)^2 \left(\frac{V_c(r)}{\text{km s}^{-1}} \right) \left(\frac{M_{\text{gc}}}{10^5 M_{\odot}} \right)^{-1} f_e. \quad (16)$$

Here V_c is the circular velocity in the Galaxy, and $f_e = 0.5$ is a correction for eccentric GC orbits [54].

As mentioned above, clusters can lose their mass due to stellar evolution (winds), star ejections after close encounters, and tidal stripping in the Galaxy. To model the mass loss due to stellar evolution, we sample stellar masses from the Kroupa initial mass function of Eq. (9), which we evolve using SSE assuming that $\bar{Z} = 0.05 Z_{\odot}$ (the average metallicity in the Harris catalog). This allows us to obtain remnant masses as a function of initial main-sequence masses (see also [65]). Thus, the mass lost via stellar evolution is simply due to the mass of the stars that evolved out of their main sequence to form compact remnants. We parametrize the typical timescale of the mass loss due to star ejections as [54]

$$t_{\text{ej}} \approx 17 \text{ Gyr} \left(\frac{M_{\text{gc}}}{2 \times 10^5 M_{\odot}} \right) \quad (17)$$

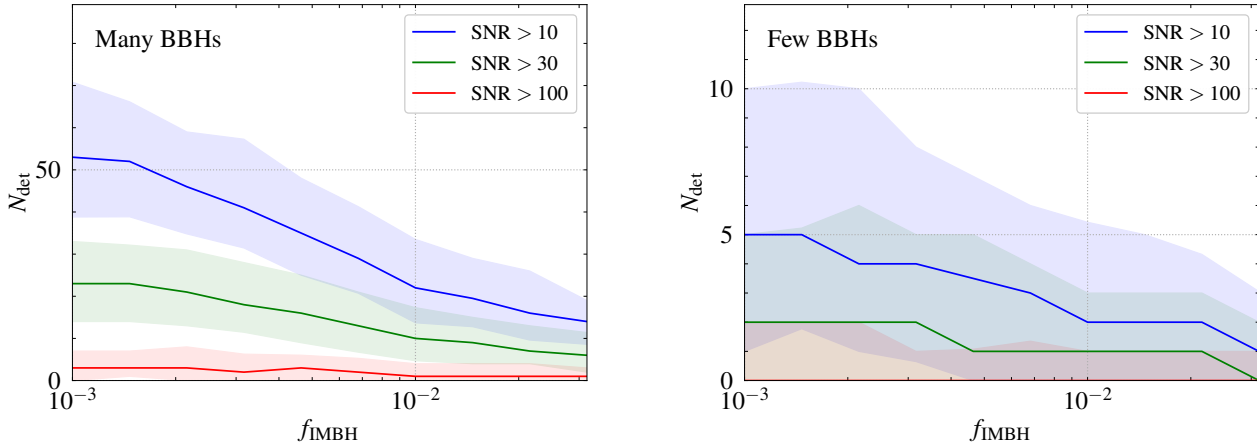


FIG. 2. Total number of detectable Doppler shift events in the Milky Way’s GCs, N_{det} , as a function of the ratio of IMBH mass to the mass of its host cluster, f_{IMBH} , in the case of many BBHs (left panel) and few BBHs (right panel). Different colors represent different values of the SNR threshold (blue: SNR > 10; green: SNR > 30; red: SNR > 100). Shaded areas indicate statistical uncertainties (95-percent quantiles).

and the timescale of tidal stripping as [66]

$$t_{\text{tid}} \approx 10 \text{ Gyr} \left(\frac{M_{\text{gc}}}{2 \times 10^5 M_{\odot}} \right)^{2/3} P(r),$$

$$P(r) = 100 \left(\frac{r}{\text{kpc}} \right) \left(\frac{V_c(r)}{\text{km s}^{-1}} \right)^{-1}. \quad (18)$$

To evolve the mass of a given GC, we first calculate the time steps at which stars in the cluster leave the main sequence. At each time step, the mass decreases by an amount equal to the difference between the mass of the star which is leaving the main sequence and the corresponding remnant mass. In between steps, the evolution of the cluster mass is governed by the equation

$$\frac{dM_{\text{GC}}}{dt} = -M_{\text{GC}} \left(\frac{1}{t_{\text{ej}}} + \frac{1}{t_{\text{tid}}} \right). \quad (19)$$

If a cluster approaches the Galactic center, we assume that it is disrupted as soon as the local Galactic density $\rho(r)$ exceeds the average density of the cluster at the half-mass radius [54], $\rho(r) > \rho_h$, eventually leaving behind the central IMBH and any BBHs orbiting it. We evolve the clusters for 10 Gyr and find that about 200 clusters survive, $\sim 10,000$ clusters get disrupted, and a few dozens of the disrupted clusters end up within 10 pc of the Galactic center. The mass distribution and Galactic density of surviving clusters is consistent with the Harris catalog [54, 66].

The number and masses of the wandering IMBHs left behind by the disrupted clusters are uncertain. For an upper bound, we assume that every GC hosted an IMBH, whose mass is a fraction of the initial mass of the cluster. As in the previous section, we consider a range of fractions $f_{\text{IMBH}} = 10^{-3} - 10^{-1.5}$, as long as the resulting IMBH mass is greater than $100M_{\odot}$. This prescription results

in ≈ 800 – $10,000$ wandering IMBHs in the Milky Way, with the number and mass distribution of these IMBHs depending on the assumed initial mass fraction.

The number of BBHs that orbit a wandering IMBH is uncertain. To estimate the number of detectable Doppler shift events, we simply assume that there is exactly one equal-mass BBH around each wandering IMBH. We consider two values of the BBH masses, motivated by the least and most massive SBHs produced from the stellar initial mass function of Eq. (9), namely $m_1 = m_2 = 10M_{\odot}$ and $m_1 = m_2 = 50M_{\odot}$ ². We sample the orbital semi-major axis of the BBH from a uniform distribution with upper limit set by the influence radius of the wandering IMBH R_{hs} , determined from

$$\frac{GM_{\text{IMBH}}(m_1 + m_2)}{R_{\text{hs}}} = 0.5 \langle m_{\star} \rangle \sigma^2(r), \quad (20)$$

where $\langle m_{\star} \rangle \approx 0.5M_{\odot}$ is the average stellar mass (assuming a canonical stellar initial mass function) and $\sigma(r)$ is the local Galactic velocity dispersion. To calculate the velocity dispersion, we use the Galactic mass profile described above and solve the Jeans equation. We have checked that the profile of $\sigma(r)$ obtained in this way is consistent with current data (see e.g. [67, 68]). The other parameters that describe the BBHs are generated as described in Sec. III A.

Our estimates for the number of BBHs orbiting wandering IMBHs and producing detectable Doppler shifts are reported in Sec. IV B below.

² These limiting masses may correspond to different metallicity; see for example Fig. 1 in Ref. [15].

TABLE I. Number of detectable events N_{det} in the case of IMBHs at the center of GCs for selected values of f_{IMBH} , as defined in Eq. (8), and of the SNR threshold.

Many BBHs			
f_{IMBH}	SNR > 10	SNR > 30	SNR > 100
0.001	53^{+18}_{-14}	23^{+10}_{-9}	3^{+4}_{-3}
0.01	22^{+12}_{-8}	10^{+7}_{-5}	1^{+3}_{-1}
Few BBHs			
f_{IMBH}	SNR > 10	SNR > 30	SNR > 100
0.001	5^{+5}_{-4}	2^{+3}_{-2}	0^{+2}_{-0}
0.01	2^{+4}_{-2}	1^{+2}_{-1}	0^{+1}_{-0}

IV. RESULTS

In this section we present the results from our simulations. We first discuss the distribution of IMBHs in Galactic GCs that can be detected via Doppler shift (Sec. IV A) and then we estimate the number of detectable IMBHs wandering in the Galaxy, left behind as a result of the disruption of their parent clusters (Sec. IV B).

In both cases we define a detectable Doppler shift event as a LISA observation such that the relative errors $\Delta v_{\parallel}/v_{\parallel}$ and $\Delta P/P$ are both smaller than 0.1 (this value is somewhat arbitrary, but it was chosen as a proxy for sufficiently precise measurements) for three selected values of the SNR threshold, namely 10, 30, and 100. Note, however, that in most cases $\Delta v_{\parallel}/v_{\parallel} \gg \Delta P/P$, so the velocity measurement is usually the limiting factor.

A. Events from the Milky Way globular clusters

In Fig. 2 we show the total number of detectable Doppler shift events N_{det} as a function of f_{IMBH} for the cases of many BBHs (left panel) and few BBHs (right panel). We report N_{det} for three selected values of the SNR threshold, namely 10, 30, and 100. We find that N_{det} decreases as a function of f_{IMBH} , i.e., N_{det} is smaller for larger IMBH masses. This can be explained considering that more massive IMBHs have larger influence radii, which leads to longer periods of BBHs around the IMBHs: see Eqs. (10) and (4). As the periods exceed the LISA mission duration, it is increasingly difficult to measure the velocity and period, and the measurement errors grow (see Fig. 2 of Ref. [33] for the dependence of the errors on the period).

In Table I we list N_{det} for the same three values of the SNR threshold listed above (10, 30, and 100) and for two selected values of $f_{\text{IMBH}} = 0.001, 0.01$. The entries in the Table can be thought of as two vertical “cuts” in the left and right panels of Fig. 2.

In Fig. 3 we further break down the results of our

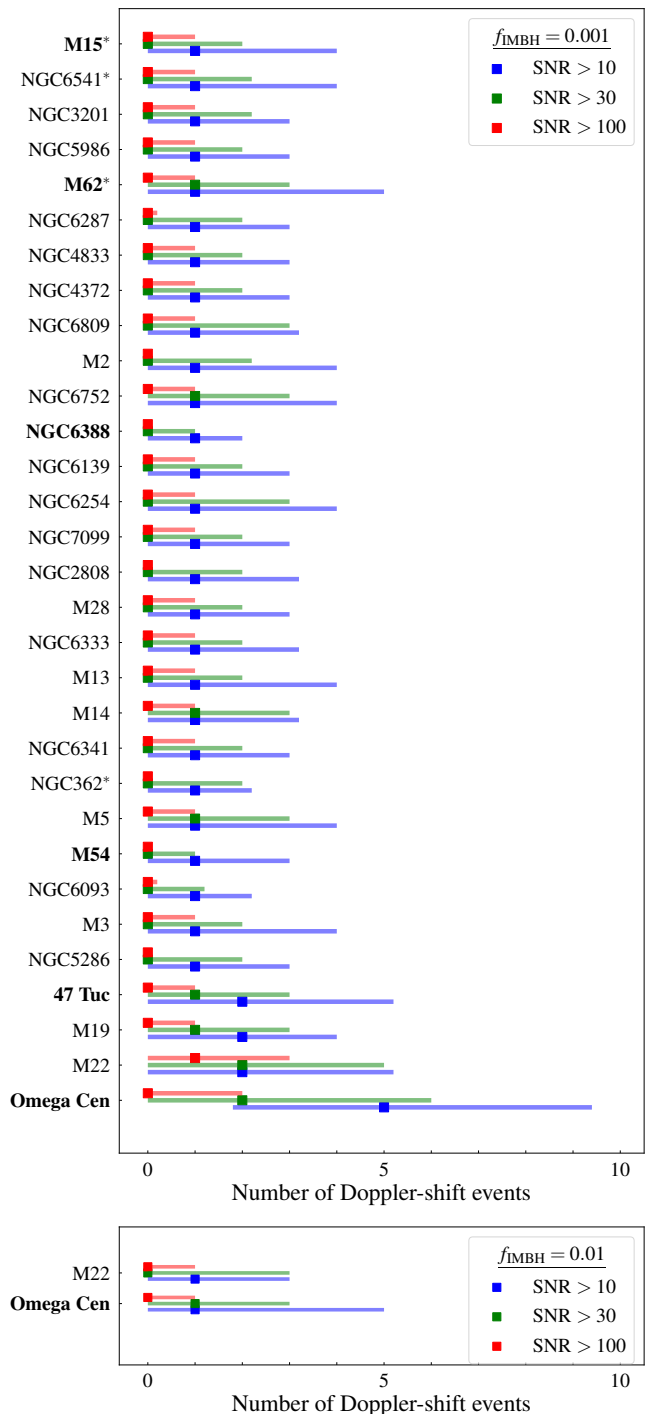


FIG. 3. Total number of Doppler shift events in individual clusters for $f_{\text{IMBH}} = 0.001$ (top) and $f_{\text{IMBH}} = 0.01$ (bottom) for three different values of the SNR threshold (blue: SNR > 10; green: SNR > 30; red: SNR > 100) in the case of many BBHs (see Sec. III A). The plots include only GCs with a median value of one or more events with SNR > 10. The horizontal bars indicate statistical uncertainties (95-percent quantiles) around the median. Clusters with observational constraints on the IMBH mass (see Table 3 in Ref. [4]) are highlighted in bold. Asterisks mark GCs that are core-collapsed according to the 2010 edition of the Harris catalog [45].

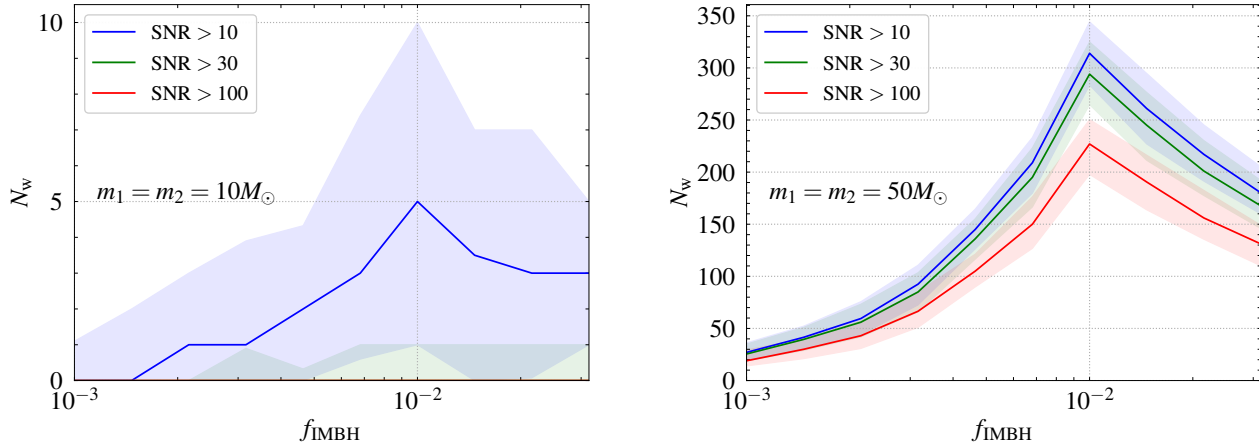


FIG. 4. Total number of Doppler shift events around wandering IMBHs as a function of f_{IMBH} for equal-mass BBHs with individual component masses of $10M_{\odot}$ (left) and $50M_{\odot}$ (right) and three different SNR thresholds (blue: SNR > 10; green: SNR > 30; red: SNR > 100). Shaded areas indicate statistical uncertainties (95-percent quantiles). Note that f_{IMBH} is the ratio of IMBH mass to the initial mass of its destroyed parent cluster.

simulations by listing the most promising Galactic GCs that could yield detectable Doppler shift events. We focus, for concreteness, on the case of many BBHs. The top and bottom panels refer to $f_{\text{IMBH}} = 0.001$ and $f_{\text{IMBH}} = 0.01$, respectively. Both panels include only GCs yielding a median of one or more events with SNR > 10. The median values, as well as the statistical uncertainties, are based on an ensemble of 112 simulation runs for each value of f_{IMBH} .

Let us focus on $f_{\text{IMBH}} = 0.001$ first (top panel). We find in total 31 Galactic GCs yielding at least a median of one event at SNR > 10. Out of these GCs, 4 (47 Tucanae, M19, M22, and ω Centauri) yield 2 events or more.

Some of the GCs in the list (NGC6388, M15, M62, M54, 47 Tucanae, and ω Centauri) could harbor IMBHs with estimated masses of $\lesssim 10^3M_{\odot}$ – 10^4M_{\odot} , $\lesssim 1,500M_{\odot}$ – $3,000M_{\odot}$, $\lesssim 1,000M_{\odot}$ – $3,000M_{\odot}$, $\lesssim 10,000M_{\odot}$, $\lesssim 2,000M_{\odot}$, and $\lesssim 10^3M_{\odot}$ – 10^4M_{\odot} , respectively (see Table 3 in Ref. [4]). The putative IMBH in these GCs can account for at most $\sim 0.1\%$ – 1% of the cluster mass, making these clusters good candidates for Doppler shift events. Note however that M15 and M62 (marked with an asterisk in Fig. 3) are known to be core-collapsed clusters, thus they are likely to contain few SBHs (see e.g. [69]), rendering the detection of a Doppler shift event less likely.

The best candidate is represented by ω Centauri, the most massive of the Milky Way’s GCs. For this GC, we predict 5_{-3}^{+5} and 2_{-2}^{+4} events at SNR > 10 and SNR > 30, respectively. Note that ω Centauri could harbor an IMBH with mass $\lesssim 10^3M_{\odot}$ – 10^4M_{\odot} (corresponding to $f_{\text{IMBH}} \lesssim 10^{-3}$ – 10^{-2}) and it is not core-collapsed, so it may host a relatively abundant population of SBHs (see e.g. [59]).

We now turn to $f_{\text{IMBH}} = 0.01$ (Fig. 3, bottom panel), where we are still considering the case of many BBHs.

There are now only 2 GCs with 1+ Doppler shift events observable at SNR > 10. Both of these GCs (ω Centauri and M22) also appear on the top panel of Fig. 3, and they include 1 GC with an IMBH candidate: ω Centauri, our most promising target, which now yields 1_{-1}^{+4} and 1_{-1}^{+2} at SNR > 10 and SNR > 30, respectively.

In both the top and bottom panels, the median values for SNR > 100 are mostly zero. However, all of our results should be understood as statistical averages (recall that each simulation ensemble comprises 112 runs). The nonvanishing error bars indicate that events with such high SNRs could still be observed. The median values fluctuate between different simulation ensembles. Due to these statistical fluctuations, at least one GC (M22) can yield a number of detections compatible with one, and in some of our runs two of the GCs (M19 and 47 Tucanae) happened to appear also in the bottom panel of Fig. 3.

Let us close this discussion with some remarks on the case of few BBHs, which was not shown in Fig. 3. In this more pessimistic scenario we find only a handful of GCs having ~ 1 event with SNR > 10: only a few GCs, if any, would have detectable Doppler shift events. The formal median values are now zero for all GCs considered, but the error bars may allow for up to 2 events.

B. Events from wandering intermediate-mass black holes

In Fig. 4 we plot estimates for the total number of Doppler shift events N_w for wandering IMBHs as a function of f_{IMBH} . Note that in this case f_{IMBH} is the ratio of the IMBH mass to the initial mass of its destroyed parent cluster. We assume that exactly one BBH orbits around each wandering IMBH at any given time (see

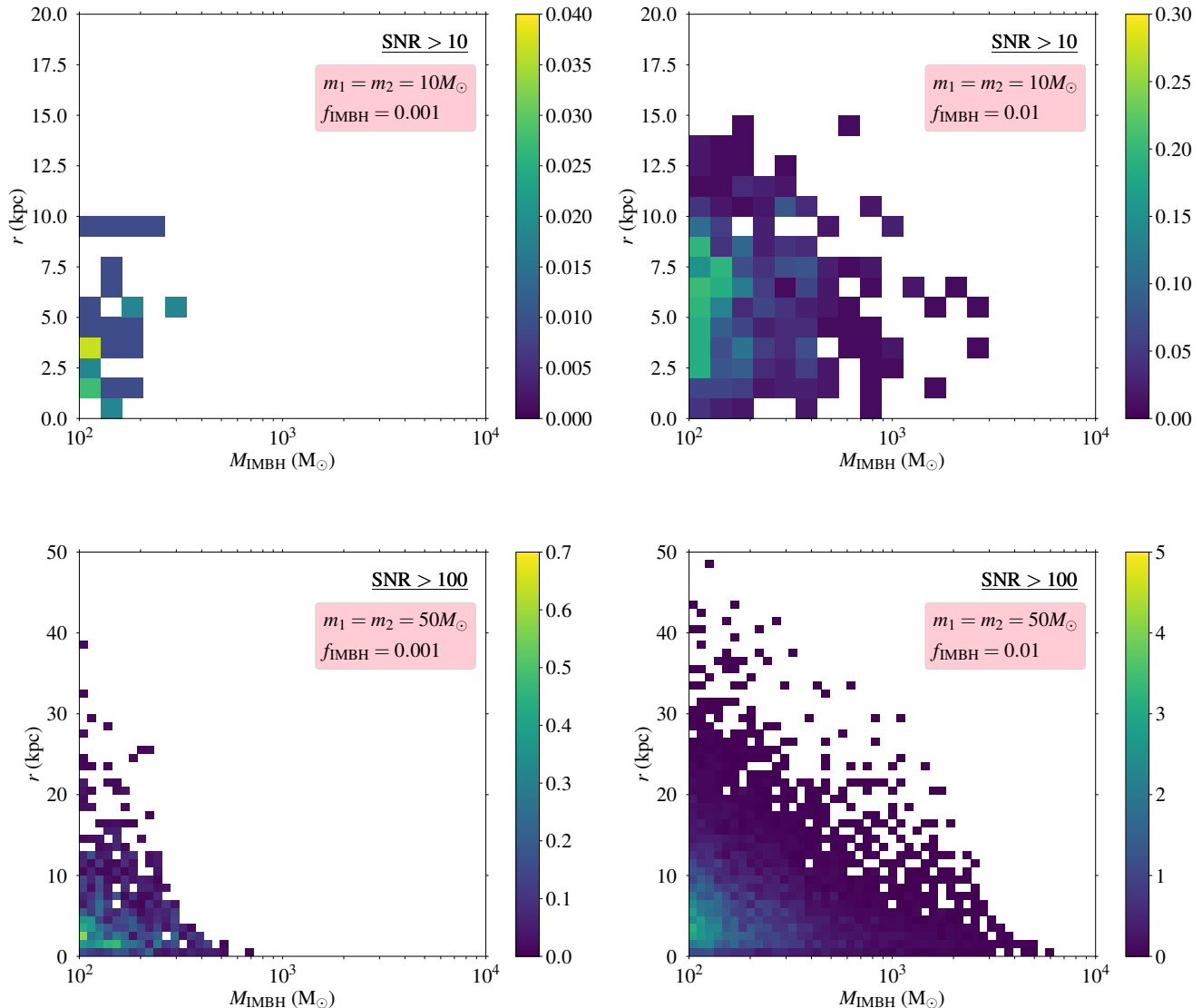


FIG. 5. Distribution of the number of Doppler shift events around individual wandering IMBHs as a function of the mass of the wandering IMBH and the distance from the Galactic center for $f_{\text{IMBH}} = 0.001$ (left) and $f_{\text{IMBH}} = 0.01$ (right). The number of events is calculated over 112 simulation runs. The top panels refer to light BBHs ($m_1 = m_2 = 10M_\odot$) and a threshold $\text{SNR} > 10$, because higher SNR thresholds yield almost no events (see Table II). The bottom panels refer to heavy BBHs ($m_1 = m_2 = 50M_\odot$) and $\text{SNR} > 100$, because the distributions for lower SNR thresholds look qualitatively similar. Note also the different ranges of the color-coded scales.

Sec. III B). The two panels refer to the cases of light ($m_1 = m_2 = 10M_\odot$, left) and heavy ($m_1 = m_2 = 50M_\odot$, right) BBHs. As before, we report N_{det} for three selected SNR thresholds: 10, 30, and 100.

The trend is different from the case of the Milky Way’s GCs: now N_w increases for $10^{-3} < f_{\text{IMBH}} < 10^{-2}$, and it decreases for $f_{\text{IMBH}} > 10^{-2}$. This can be explained as follows. The majority of primordial GCs have initial masses $\sim 10^4 M_\odot$ as a result of the negative slope of the GC initial mass function: see Eq. (14). Since they are not massive and dense enough to survive until now, most of these clus-

ters are disrupted by the Galactic tidal field. However, no IMBHs will be left behind for $f_{\text{IMBH}} < 10^{-2}$, since this would correspond to IMBH masses $< 100 M_\odot$. Therefore the number of events increases for $f_{\text{IMBH}} < 10^{-2}$, since more and more disrupted GCs leave behind IMBHs with masses $> 100 M_\odot$. For example, the disruption of GCs produces ~ 100 wandering IMBHs heavier than $100 M_\odot$ in the Galaxy for $f_{\text{IMBH}} \approx 10^{-3}$, while almost every disrupted GC will leave behind an IMBH for $f_{\text{IMBH}} \approx 10^{-2}$. Beyond the peak at $f_{\text{IMBH}} > 10^{-2}$ the number of Doppler shift events decreases, since more massive IMBHs have

TABLE II. Number of detectable events N_w around wandering IMBHs for selected values of f_{IMBH} , as defined in Eq. (8), and of the SNR threshold.

$m_1 = m_2 = 10M_\odot$			
f_{IMBH}	SNR > 10	SNR > 30	SNR > 100
0.001	0_{-0}^{+2}	0	0
0.01	5_{-3}^{+5}	0_{-0}^{+1}	0
$m_1 = m_2 = 50M_\odot$			
f_{IMBH}	SNR > 10	SNR > 30	SNR > 100
0.001	26_{-9}^{+9}	25_{-8}^{+7}	19_{-7}^{+8}
0.01	297_{-30}^{+32}	276_{-29}^{+32}	214_{-24}^{+27}

both larger tidal radii and larger influence radii (see the discussion in Sec. IV A).

In Table II we report the total number of Doppler shift events N_w around wandering IMBHs in the Galaxy for the three values of SNR (10, 30, and 100) and two values of $f_{\text{IMBH}} = 0.001, 0.01$. As explained above, the number of events is largest for $f_{\text{IMBH}} = 0.01$. It is also larger (as expected) for the case of BBHs with heavy components $m_1 = m_2 = 50M_\odot$, which generate a stronger GW signal. In this case, we find that ~ 10 and ~ 100 Doppler shift events could be detectable for $f_{\text{IMBH}} = 0.001$ and 0.01, respectively.

Fig. 5 shows the distribution of the number of Doppler shift events as a function of the masses of wandering IMBHs and their distances from the Galactic center. The top and bottom rows correspond to the light and heavy BBH cases, while the left and right columns refer to $f_{\text{IMBH}} = 0.001$ and $f_{\text{IMBH}} = 0.01$, respectively. In the case of light BBHs we only show the distribution for SNR > 10, because the number of events practically vanishes at the higher SNR thresholds. In the case of heavy BBHs we only show the distribution for SNR > 100, because the distributions for different SNR thresholds are qualitatively similar. The heat maps are weighted by the probability for an event to occur. More precisely, we run our simulation 112 times for each wandering IMBH and each combination of parameters (SNR, f_{IMBH} , and the component masses). Then we divide the number of simulation runs that resulted in an event by 112 to obtain the probability for an event with the given parameters to occur. Thus, all numbers smaller than unity in the heat maps can be interpreted as the probability for an event to occur. The number of simulation runs also gives a lower bound of $\approx 1\%$ on this probability, since the heat maps are based on 112 runs. Typical probabilities are in the range 1%–10%.

The heat maps illustrate three trends.

First, the events clearly cluster at a distance of a few kpc from the Galactic center. The overall clustering of the wandering IMBHs towards the center is not unexpected:

TABLE III. Approximate numbers of detectable events N_w around wandering IMBHs within a distance r from the Galactic center for selected values of f_{IMBH} , as defined in Eq. (8). A fractional number of events should be interpreted as a probability of detection during the LISA mission.

$m_1 = m_2 = 10M_\odot$			
f_{IMBH}	$r < 5$ kpc	$r < 10$ kpc	$r < 20$ kpc
0.001	0.2	0.3	0.3
0.01	2	4	5
$m_1 = m_2 = 50M_\odot$			
f_{IMBH}	$r < 5$ kpc	$r < 10$ kpc	$r < 20$ kpc
0.001	12	17	19
0.01	110	180	210

the primordial distribution of Galactic GCs follows the Galactic density profile, and GCs are more likely to be disrupted near the center of the Milky Way, leaving behind wandering IMBHs. The events cluster at some finite distance from the center, approximately corresponding to the distance at which the Milky Way velocity dispersion has a maximum. This is because larger dispersion results in smaller influence radii for the wandering IMBHs [cf. Eq. (20)], which in turn leads to tighter orbits of BBHs around the IMBHs and to shorter orbital periods, comparable to the observation time $T_{\text{obs}} = 4$ years. This makes it easier to measure Doppler shift modulations. In Table III we provide specific approximate numbers of events within distance $r = 5$ kpc, 10 kpc, and 20 kpc from the Galactic center. In addition, Fig. 6 illustrates the distribution of the events on the sky in equatorial coordinates. The dashed line corresponds to the Galactic plane, and the filled black circle marks the Galactic center. Note that in our simulations the primordial GCs which host the IMBHs before being disrupted are isotropically distributed in the Galaxy. The map shows a random sample of events for the case of heavy BBHs, $f_{\text{IMBH}} = 0.001$, and at the three SNR thresholds.

The second trend visible in Fig. 5 is that there are more events around lighter IMBHs. This is purely due to the large number of light IMBHs left behind by relatively light GCs, which are more prone to destruction and also more abundant, as a consequence of the bottom-heavy initial mass function of Eq. (14).

Finally, Fig. 5 demonstrates that events around heavier IMBHs are more likely to occur closer to the Galactic center. This is because heavier GCs are more likely to be destroyed and leave behind heavier IMBHs when they are close to the center. To be more quantitative, in Table IV we report estimates for the number of events around IMBHs in specific mass ranges: 100–300 M_\odot , 300–1,000 M_\odot , and 1,000–3,000 M_\odot .

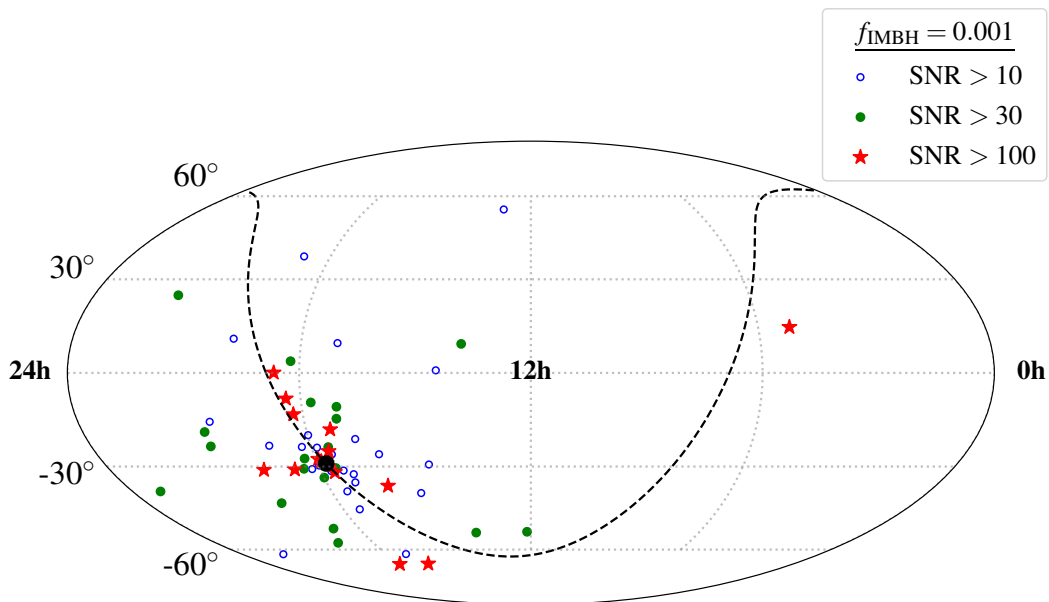


FIG. 6. Sample distribution of Doppler shift events around wandering IMBHs on the sky in equatorial coordinates. Here we consider BBHs with component masses $m_1 = m_2 = 50M_\odot$, $f_{\text{IMBH}} = 0.001$, and three values of the SNR threshold (blue empty dots: $\text{SNR} > 10$; green filled dots: $\text{SNR} > 30$; red stars: $\text{SNR} > 100$). The distribution of events on the sky for other values of the component masses and f_{IMBH} is qualitatively the same. The Galactic plane is shown with a dashed line, while the filled black circle marks the Galactic center.

TABLE IV. Approximate numbers of detectable events N_w around wandering IMBHs in three IMBH mass ranges and for selected values of f_{IMBH} , as defined in Eq. (8). A fractional number of events should be interpreted as a probability of detection during the LISA mission.

$m_1 = m_2 = 10M_\odot$			
f_{IMBH}	100–300 M_\odot	300–1,000 M_\odot	1,000–3,000 M_\odot
0.001	0.3	0.	0.
0.01	4	0.8	0.1
$m_1 = m_2 = 50M_\odot$			
f_{IMBH}	100–300 M_\odot	300–1,000 M_\odot	1,000–3,000 M_\odot
0.001	18	1	0
0.01	170	35	5

V. DISCUSSION

Finding IMBHs and characterizing their properties is of crucial importance since they play an important role in a wide range of phenomena, including seeds of massive black holes, accretion, tidal disruption events, and GWs. Despite major observational efforts IMBHs still remain elusive, and new methods are needed to detect them.

We have investigated the possibility that LISA may find

IMBHs lurking in Galactic GCs by measuring the radial velocity modulations in the GW signal of BBHs orbiting around them. We have found that the number of Doppler shift events decreases for larger IMBH masses, because more massive IMBHs have a larger influence radius and larger tidal radii. Since tidal stability requires BBHs to orbit far away from the IMBH, the Doppler modulations in their gravitational waveforms are harder to detect. We have also estimated that ~ 30 Galactic GCs could produce at least one Doppler event detectable by LISA if an IMBH lurks in their center. Among these candidate Galactic GCs, M15, M62, NGC6388, M54, and 47 Tucanae may harbor an IMBH. The best candidate in our analysis is ω Centauri, if indeed it hosts an IMBH with mass $\lesssim 10^4 M_\odot$, as suggested by dynamical measurements [4].

We have also considered the possibility of hunting for wandering Galactic IMBHs left behind by the disruption of the parent cluster. Assuming that each of these wandering IMBHs has at least one BBH orbiting around it, LISA could detect tens of Doppler events with $\text{SNR} > 10$.

In our simulations we have assumed that all Galactic GCs harbor an IMBH, whose mass is a fraction f_{IMBH} of the cluster mass, and host $\mathcal{O}(100)$ (many) or $\mathcal{O}(10)$ (few) BBHs. However, observational and theoretical evidence makes some of the GCs more promising targets than others for our present purpose. The modeling of stellar orbits close to the cluster center suggests that some Galactic GCs could indeed host an IMBH (see Table 3 in Ref. [4] for a summary). Moreover, recent numerical

models have shown that a higher degree of mass segregation in a cluster is linked to a less abundant population of SBHs [59]. This implies that GCs observationally classified as core-collapsed are likely to contain either fewer BBHs than those that have not undergone the core collapse yet [59, 69], or no BBHs at all.

Our astrophysical models are affected by several uncertain assumptions. One of the most notable uncertainties is in the distribution of BBH orbital parameters in the presence of an IMBH in GCs. In particular, the minimum semi-major axis for BBHs ($a_{\min} = 0.01$ AU in this work) plays an important role in our estimates. We have assumed for simplicity that BBH have circular orbits, but nonzero eccentricities could increase the GW amplitude of the signals and yield more optimistic rate estimates [70]. Finally, we have considered only BBHs, neglecting black hole-neutron stars binaries and binary neutron stars as possible sources of Doppler shift events. This assumption is quite well justified: these two populations of compact object binaries would likely contribute much less than BBHs, because most of the neutron stars should be ejected as a result of natal kicks and do not efficiently segregate in the cluster center, close to the central IMBHs [71–73]. These uncertainties should be better quantified through further work. Our initial estimates suggest that LISA may detect tens of Doppler shift events, thus mapping

the elusive population of IMBHs in the Milky Way.

ACKNOWLEDGMENTS

V.S., T.H. K.W.K.W. and E.B. were supported by NSF Grants No. PHY-1912550 and AST-2006538, NASA ATP Grants No. 17-ATP17-0225 and 19-ATP19-0051, NSF-XSEDE Grant No. PHY-090003, and NSF Grant PHY-20043. V.S., T.H., G.F. and E.B. are supported by NASA Grant 20-LPS20-0011. G.F. acknowledges support from NSF Grant AST-1716762 at Northwestern University. K.W.K.W. is supported by the Simons Foundation. G.F. is grateful to Sambaran Banerjee for insightful discussions on stellar evolution and for updating SSE, and to Oleg Gnedin for useful discussions on star cluster evolution. This research project was conducted using computational resources at the Maryland Advanced Research Computing Center (MARCC). The authors acknowledge the Texas Advanced Computing Center (TACC) at The University of Texas at Austin for providing HPC resources that have contributed to the research results reported within this paper [74] (URL: <http://www.tacc.utexas.edu>). This research made use of the following software: IPython [75], SciPy [76], Matplotlib [77], NumPy [78], SymPy [79], mpmath [44], filltex [80].

-
- [1] V. F. Baldassare, M. Geha, and J. Greene, *ApJ* **868**, 152 (2018), [arXiv:1808.09578](https://arxiv.org/abs/1808.09578) [astro-ph.GA].
 - [2] I. V. Chilingarian, I. Y. Katkov, I. Y. Zolotukhin, K. A. Grishin, Y. Beletsky, K. Boutsia, and D. J. Osip, *ApJ* **863**, 1 (2018), [arXiv:1805.01467](https://arxiv.org/abs/1805.01467) [astro-ph.GA].
 - [3] D. Lin, J. Strader, E. R. Carrasco, D. Page, A. J. Romanowsky, J. Homan, J. A. Irwin, R. A. Remillard, O. Godet, N. A. Webb, H. Baumgardt, R. Wijnands, D. Barret, P.-A. Duc, J. P. Brodie, and S. D. J. Gwyn, *Nature Astronomy* **2**, 656 (2018), [arXiv:1806.05692](https://arxiv.org/abs/1806.05692) [astro-ph.HE].
 - [4] J. E. Greene, J. Strader, and L. C. Ho, *Annual Review of Astronomy and Astrophysics* **58**, 257 (2020).
 - [5] M. J. Rees, *The Observatory* **98**, 210 (1978).
 - [6] A. Loeb and F. A. Rasio, *ApJ* **432**, 52 (1994), [arXiv:astro-ph/9401026](https://arxiv.org/abs/astro-ph/9401026) [astro-ph].
 - [7] V. Bromm and A. Loeb, *ApJ* **596**, 34 (2003), [arXiv:astro-ph/0212400](https://arxiv.org/abs/astro-ph/0212400) [astro-ph].
 - [8] P. Madau and M. J. Rees, *ApJ* **551**, L27 (2001), [arXiv:astro-ph/0101223](https://arxiv.org/abs/astro-ph/0101223) [astro-ph].
 - [9] V. Bromm and R. B. Larson, *ARA&A* **42**, 79 (2004), [arXiv:astro-ph/0311019](https://arxiv.org/abs/astro-ph/0311019) [astro-ph].
 - [10] C. L. Fryer, S. E. Woosley, and A. Heger, *ApJ* **550**, 372 (2001), [arXiv:astro-ph/0007176](https://arxiv.org/abs/astro-ph/0007176) [astro-ph].
 - [11] S. F. Portegies Zwart and S. L. W. McMillan, *ApJ* **576**, 899 (2002), [arXiv:astro-ph/0201055](https://arxiv.org/abs/astro-ph/0201055) [astro-ph].
 - [12] M. A. Gürkan, M. Freitag, and F. A. Rasio, *ApJ* **604**, 632 (2004), [arXiv:astro-ph/0308449](https://arxiv.org/abs/astro-ph/0308449) [astro-ph].
 - [13] M. Giersz, N. W. Leigh, A. Hypki, N. Lützgendorf, and A. Askar, *MNRAS* **454**, 3150 (2015).
 - [14] F. Antonini, M. Gieles, and A. Gualandris, *MNRAS* **486**, 5008 (2019), [arXiv:1811.03640](https://arxiv.org/abs/1811.03640) [astro-ph.HE].
 - [15] G. Fragione, A. Loeb, and F. A. Rasio, *ApJ* **902**, L26 (2020), [arXiv:2009.05065](https://arxiv.org/abs/2009.05065) [astro-ph.GA].
 - [16] G. Fragione and J. Silk, *MNRAS* **498**, 4591 (2020), [arXiv:2006.01867](https://arxiv.org/abs/2006.01867) [astro-ph.GA].
 - [17] G. Fragione, B. Kocsis, F. A. Rasio, and J. Silk, *arXiv e-prints*, [arXiv:2107.04639](https://arxiv.org/abs/2107.04639) (2021), [arXiv:2107.04639](https://arxiv.org/abs/2107.04639) [astro-ph.GA].
 - [18] E. González, K. Kremer, S. Chatterjee, G. Fragione, and et al., *ApJ* **908**, L29 (2021), [arXiv:2012.10497](https://arxiv.org/abs/2012.10497) [astro-ph.HE].
 - [19] M. Mapelli, M. Dall’Amico, Y. Bouffanais, N. Giacobbo, and et al., *MNRAS* **505**, 339 (2021), [arXiv:2103.05016](https://arxiv.org/abs/2103.05016) [astro-ph.HE].
 - [20] J. E. Greene and L. C. Ho, *ApJ* **670**, 92 (2007), [arXiv:0707.2617](https://arxiv.org/abs/0707.2617) [astro-ph].
 - [21] P. Kaaret, H. Feng, and T. P. Roberts, *ARA&A* **55**, 303 (2017), [arXiv:1703.10728](https://arxiv.org/abs/1703.10728) [astro-ph.HE].
 - [22] A. Gualandris, S. Gillessen, and D. 2013degn.book.....M, *MNRAS* **409**, 1146 (2010), [arXiv:1006.3563](https://arxiv.org/abs/1006.3563) [astro-ph.GA].
 - [23] H. Baumgardt, C. He, S. M. Sweet, M. Drinkwater, A. Sollima, J. Hurley, C. Usher, S. Kamann, H. Dalgleish, S. Dreizler, and T. O. Husser, *MNRAS* **488**, 5340 (2019), [arXiv:1907.10845](https://arxiv.org/abs/1907.10845) [astro-ph.GA].
 - [24] E. Girma and A. Loeb, *MNRAS* **482**, 3669 (2019), [arXiv:1807.02469](https://arxiv.org/abs/1807.02469) [astro-ph.GA].
 - [25] G. Fragione, N. W. C. Leigh, I. Ginsburg, and B. Kocsis, *ApJ* **867**, 119 (2018), [arXiv:1806.08385](https://arxiv.org/abs/1806.08385) [astro-ph.GA].
 - [26] P. Amaro-Seoane, J. R. Gair, M. Freitag, M. C. Miller, I. Mandel, C. J. Cutler, and S. Babak, *Classical and Quan-*

- tum Gravity **24**, R113 (2007), [arXiv:astro-ph/0703495 \[astro-ph\]](#).
- [27] C. Cutler, E. Berti, K. Holley-Bockelmann, K. Jani, E. D. Kovetz, S. L. Larson, T. Littenberg, S. T. McWilliams, G. Mueller, L. Randall, J. D. Schnittman, D. H. Shoemaker, M. Vallisneri, S. Vitale, and K. W. K. Wong, *BAAS* **51**, 109 (2019), [arXiv:1903.04069 \[astro-ph.HE\]](#).
- [28] M. Arca Sedda, C. P. L. Berry, K. Jani, P. Amaro-Seoane, P. Auclair, J. Baird, T. Baker, E. Berti, K. Breivik, A. Burrows, C. Caprini, X. Chen, D. Doneva, J. M. Ezquiaga, K. E. Saavik Ford, M. L. Katz, S. Kolkowitz, B. McKernan, G. Mueller, G. Nardini, I. Pikovski, S. Rajendran, A. Sesana, L. Shao, N. Tamanini, D. Vartanyan, N. Warburton, H. Witek, K. Wong, and M. Zevin, *Classical and Quantum Gravity* **37**, 215011 (2020), [arXiv:1908.11375 \[gr-qc\]](#).
- [29] I. Mandel, D. A. Brown, J. R. Gair, and M. C. Miller, *ApJ* **681**, 1431 (2008), [arXiv:0705.0285 \[astro-ph\]](#).
- [30] G. Fragione, I. Ginsburg, and B. Kocsis, *ApJ* **856**, 92 (2018).
- [31] A. Rasskazov, G. Fragione, and B. Kocsis, *The Astrophysical Journal* **899**, 149 (2020).
- [32] R. Abbott et al., *Physical Review Letters* **125**, 10.1103/physrevlett.125.101102 (2020).
- [33] K. W. K. Wong, V. Baibhav, and E. Berti, *Monthly Notices of the Royal Astronomical Society* **488**, 5665 (2019).
- [34] K. Inayoshi, N. Tamanini, C. Caprini, and Z. Haiman, *Phys. Rev. D* **96**, 063014 (2017), [arXiv:1702.06529 \[astro-ph.HE\]](#).
- [35] C. Bonvin, C. Caprini, R. Sturani, and N. Tamanini, *Phys. Rev. D* **95**, 044029 (2017), [arXiv:1609.08093 \[astro-ph.CO\]](#).
- [36] N. Tamanini, A. Klein, C. Bonvin, E. Barausse, and C. Caprini, *Physical Review D* **101**, 10.1103/physrevd.101.063002 (2020).
- [37] Z. Xuan, P. Peng, and X. Chen, *MNRAS* **502**, 4199 (2021), [arXiv:2012.00049 \[astro-ph.HE\]](#).
- [38] C. Cutler, *Physical Review D* **57**, 7089 (1998).
- [39] E. Berti, A. Buonanno, and C. M. Will, *Physical Review D* **71**, 10.1103/physrevd.71.084025 (2005).
- [40] M. Vallisneri, *Physical Review D* **77**, 10.1103/physrevd.77.042001 (2008).
- [41] S. Babak, M. Hewitson, and A. Petiteau, *arXiv e-prints*, [arXiv:2108.01167 \(2021\)](#), [arXiv:2108.01167 \[astro-ph.IM\]](#).
- [42] P. Amaro-Seoane et al., *arXiv e-prints*, [arXiv:1702.00786 \(2017\)](#), [arXiv:1702.00786 \[astro-ph.IM\]](#).
- [43] P. Amaro-Seoane, M. Arca Sedda, S. Babak, C. P. L. Berry, E. Berti, G. Bertone, D. Blas, T. Bogdanović, M. Bonetti, K. Breivik, R. Brito, R. Caldwell, P. R. Capelo, C. Caprini, V. Cardoso, Z. Carson, H.-Y. Chen, A. J. K. Chua, I. Dvorkin, Z. Haiman, L. Heisenberg, M. Isi, N. Karnesis, B. J. Kavanagh, T. B. Littenberg, A. Mangiagli, P. Marcoccia, A. Maselli, G. Nardini, P. Pani, M. Peloso, M. Pieroni, A. Ricciardone, A. Sesana, N. Tamanini, A. Toubiana, R. Valiante, S. Vretinaris, D. Weir, K. Yagi, and A. Zimmerman, *arXiv e-prints*, [arXiv:2107.09665 \(2021\)](#), [arXiv:2107.09665 \[astro-ph.IM\]](#).
- [44] F. Johansson et al., *mpmath: a Python library for arbitrary-precision floating-point arithmetic (version 1.1.0)* (2013), <http://mpmath.org/>.
- [45] W. E. Harris, *AJ* **112**, 1487 (1996).
- [46] W. E. Harris, J. P. Blakeslee, and G. L. H. Harris, *ApJ* **836**, 67 (2017), [arXiv:1701.04845 \[astro-ph.GA\]](#).
- [47] D. E. McLaughlin, *The Astrophysical Journal* **539**, 618 (2000).
- [48] M. Rejkuba, P. Dubath, D. Minniti, and G. Meylan, *Astronomy & Astrophysics* **469**, 147 (2007).
- [49] H. Baumgardt, *Monthly Notices of the Royal Astronomical Society* **464**, 2174 (2016).
- [50] P. Kroupa, *Monthly Notices of the Royal Astronomical Society* **322**, 231 (2001).
- [51] J. R. Hurley, O. R. Pols, and C. A. Tout, *MNRAS* **315**, 543 (2000), [arXiv:astro-ph/0001295 \[astro-ph\]](#).
- [52] S. Banerjee, K. Belczynski, C. L. Fryer, P. Berczik, J. R. Hurley, R. Spurzem, and L. Wang, *A&A* **639**, A41 (2020), [arXiv:1902.07718 \[astro-ph.SR\]](#).
- [53] E. Anders and N. Grevesse, *Geochimica et Cosmochimica Acta* **53**, 197 (1989).
- [54] O. Y. Gnedin, J. P. Ostriker, and S. Tremaine, *ApJ* **785**, 71 (2014), [arXiv:1308.0021 \[astro-ph.CO\]](#).
- [55] R. A. Mardling and S. J. Aarseth, *MNRAS* **321**, 398 (2001).
- [56] F. Antonini and H. B. Perets, *ApJ* **757**, 27 (2012), [arXiv:1203.2938 \[astro-ph.GA\]](#).
- [57] G. Fragione, E. Grishin, N. W. C. Leigh, H. B. Perets, and et al., *MNRAS* **488**, 47 (2019), [arXiv:1811.10627 \[astro-ph.GA\]](#).
- [58] M. Morscher, B. Pattabiraman, C. Rodriguez, F. A. Rasio, and S. Umbreit, *The Astrophysical Journal* **800**, 9 (2015).
- [59] N. C. Weatherford, S. Chatterjee, K. Kremer, and F. A. Rasio, *The Astrophysical Journal* **898**, 162 (2020).
- [60] N. C. Weatherford, G. Fragione, K. Kremer, S. Chatterjee, and et al., *ApJ* **907**, L25 (2021), [arXiv:2101.02217 \[astro-ph.GA\]](#).
- [61] K. Kremer, M. Spera, D. Becker, S. Chatterjee, and et al., *ApJ* **903**, 45 (2020), [arXiv:2006.10771 \[astro-ph.HE\]](#).
- [62] T. C. Licquia and J. A. Newman, *The Astrophysical Journal* **806**, 96 (2015).
- [63] J. L. Sérsic, *Boletín de la Asociación Argentina de Astronomía La Plata Argentina* **6**, 41 (1963).
- [64] J. F. Navarro, C. S. Frenk, and S. D. M. White, *The Astrophysical Journal* **490**, 493 (1997).
- [65] M. Mapelli, *arXiv e-prints*, [arXiv:2106.00699 \(2021\)](#), [arXiv:2106.00699 \[astro-ph.HE\]](#).
- [66] G. Fragione, F. Antonini, and O. Y. Gnedin, *The Astrophysical Journal* **871**, L8 (2019).
- [67] W. Dehnen, D. E. McLaughlin, and J. Sachania, *MNRAS* **369**, 1688 (2006), [arXiv:astro-ph/0603825 \[astro-ph\]](#).
- [68] W. R. Brown, M. J. Geller, S. J. Kenyon, and A. Diaferio, *AJ* **139**, 59 (2010), [arXiv:0910.2242 \[astro-ph.GA\]](#).
- [69] K. Kremer, C. S. Ye, N. Z. Rui, N. C. Weatherford, S. Chatterjee, G. Fragione, C. L. Rodriguez, M. Spera, and F. A. Rasio, *ApJS* **247**, 48 (2020), [arXiv:1911.00018 \[astro-ph.HE\]](#).
- [70] P. C. Peters and J. Mathews, *Physical Review* **131**, 435 (1963).
- [71] G. Fragione, V. Pavlík, and S. Banerjee, *MNRAS* **480**, 4955 (2018), [arXiv:1804.04856 \[astro-ph.GA\]](#).
- [72] C. S. Ye, W.-f. Fong, K. Kremer, C. L. Rodriguez, S. Chatterjee, G. Fragione, and F. A. Rasio, *ApJ* **888**, L10 (2020), [arXiv:1910.10740 \[astro-ph.HE\]](#).
- [73] G. Fragione and S. Banerjee, *ApJ* **901**, L16 (2020), [arXiv:2006.06702 \[astro-ph.GA\]](#).
- [74] D. Stanzione, J. West, R. T. Evans, T. Minyard, O. Ghattas, and D. K. Panda, in *Practice and Experience in Advanced Research Computing*, PEARC '20 (Association for Computing Machinery, New

- York, NY, USA, 2020) p. 106–111.
- [75] F. Perez and B. E. Granger, *Computing in Science and Engineering* **9**, 21 (2007).
 - [76] P. Virtanen, R. Gommers, T. E. Oliphant, M. Haberland, T. Reddy, D. Cournapeau, E. Burovski, P. Peterson, W. Weckesser, J. Bright, S. J. van der Walt, M. Brett, J. Wilson, K. J. Millman, N. Mayorov, A. R. J. Nelson, E. Jones, R. Kern, E. Larson, C. J. Carey, Í. Polat, Y. Feng, E. W. Moore, J. VanderPlas, D. Laxalde, J. Perktold, R. Cimrman, I. Henriksen, E. A. Quintero, C. R. Harris, A. M. Archibald, A. H. Ribeiro, F. Pedregosa, P. van Mulbregt, and SciPy 1.0 Contributors, *Nature Methods* **17**, 261 (2020), arXiv:1907.10121 [cs.MS].
 - [77] J. D. Hunter, *Computing in Science and Engineering* **9**, 90 (2007).
 - [78] S. van der Walt, S. C. Colbert, and G. Varoquaux, *Computing in Science and Engineering* **13**, 22 (2011), arXiv:1102.1523 [cs.MS].
 - [79] A. Meurer et al., *PeerJ Comput. Sci.* **3**, e103 (2017).
 - [80] D. Gerosa and M. Vallisneri, *The Journal of Open Source Software* **2**, 222 (2017).